Article

Maximizing spectral sensitivity without compromising resolution in phase-incremented, steady-state solution NMR

Mark Shif[1], Yuval Zur[2] ✉, Adonis Lupulescu[1], Tian He[1,3], Elton T. Montrazi [1] & Lucio Frydman [1] ✉

NMR acquisitions based on Ernst-angle excitations are widely used for maximizing spectral sensitivity without compromising bandwidth or resolution. However, if relaxation times T_1, T_2 are long and similar, as is often the case in liquids, steady-state free-precession (SSFP) experiments could provide higher sensitivity per $\sqrt{\text{acquisition\_time}}$ (SNR$_t$). Although strong offset dependencies and poor spectral resolutions have impeded SSFP's analytical applications, this study reexplores if, when and how can phase-incremented (PI) SSFP schemes overcome these drawbacks. It is found that PI-SSFP can indeed provide a superior SNR$_t$ than Ernst-angle FT-NMR acquisitions, but that achieving this requires using relatively large flip angles. This, however, can restrict PI-SSFP's spectral resolution and lead to distorted line shapes; to deal with this we introduce here a new SSFP outlook that overcomes this dichotomy. This outlook also leads to a new processing pipeline for PI-SSFP acquisitions, providing high spectral resolution even when utilizing relatively the large flip angles. The enhanced SNR$_t$ that the ensuing method can provide over FT-based NMR counterparts, is demonstrated with a series of ^{13}C and ^{15}N investigations on organic compounds.

Nuclear Magnetic Resonance (NMR) is an essential tool in contemporary chemistry, widely used in both academia and industry to derive molecular structures, dynamics and concentrations[1-5]. Whether carried on liquid or solid samples, whether focusing on glasses or on living organisms, nearly all NMR experiments follow Anderson-and-Ernst's Nobel-award-winning Fourier Transform (FT) proposition[1-7]. That is not surprising as FT-NMR is simple, general, and provides excellent resolution while covering large spectral bandwidths. Furthermore, and crucial in its eventual adoption as "the" way of collecting NMR data, FT-NMR exhibits better signal-to-noise ratio per $\sqrt{\text{acquisition\_time}}$ (SNR$_t$) than alternative frequency-domain-based approaches. However, it is also known that if spectral resolution and the faithful coverage of peak intensities over large bandwidths are not a must, the Anderson-Ernst FT-NMR proposal is not necessarily optimal for achieving the highest SNR$_t$: when $T_1 \approx T_2$, as is often in solution-

state experiments, and if a peak's offset and the excitation pulse angle can be chosen at will, Carr's steady-state free-precession (SSFP) NMR can often provide a superior SNR$_t$[8-10]. While instances where SSFP could become a method of choice in spectroscopic applications have been described in low-resolution and in solid-state NMR and NQR[11-14], the aforementioned limitations have constrained SSFP's use to MRI –where it is widely exploited under variety of vendor-dependent acronyms[15-17]. SNR$_t$ advantages were also here **the** defining reasons of why MRI, a widely used yet costly medical imaging modality where both scanning duration and data quality are of essence, was quick to adopt SSFP. Indeed, with a focus on a single water resonance whose offset can be chosen more-or-less at will and with T_1 and T_2 times that are reasonably close, MRI was also uniquely posed to deal with SSFP's main two drawbacks: its lack of spectral resolution, and its strong dependence on the offset (i.e., the chemical shift) of the targeted

[1]Chemical and Biological Physics Department, Weizmann Institute, Rehovot, Israel. [2]Insightec Ltd, Tirat Carmel, Israel. [3]Chemistry Department, Zhejiang University, Zhejiang, P. R. China. ✉e-mail: yuvalzur50@gmail.com; lucio.frydman@weizmann.ac.il

peaks. SSFP's spectral resolution limitations can be adumbrated from its pulse sequence, which involves a train of closely spaced pulses with constant flip-angle α, applied at repetition times $TR \ll T_2, T_1$ (Fig. 1, top). This leads to signals S(t) that are a combination of free induction decays (FIDs) and of multiple echoes –the latter reflecting, at each TR, a sum of histories associated to different coherence transfer pathways[1–4] (or as known in the MRI literature, to different extended phase diagrams[18,19]) refocusing at the top of every pulse in the sequence. SSFP's SNR_t potential and offset dependence –qualities which will both be central in this study– are highlighted in Fig. 1 (bottom). It follows from these extensively verified predictions that steady-state pulses can lead to transverse magnetizations reaching up to 50% of the thermal equilibrium magnetization, in a nearly constant emission of NMR signals. Such feat, however, requires the resonance being addressed to have a suitable, a priori known offset Δ, and the use of relatively large flip angles α. The issue of offset-dependence has been particularly detrimental in high-resolution NMR settings: given SSFP's repeated pulsing, offsets will arise (e.g., an on-resonance situation) where a steady, large-flip-angle pulsing with a constant phase (e.g., x), will lead to a null ($M_{x,y} \approx 0$) signal. Furthermore, given SSFP's periodicity, its offset-dependent excitation profile will repeat itself modulo $2\pi/TR$. When coupling to this alternating dark/bright spectral pattern the limited spectral resolution arising from its demand for short TRs, it is clear why SSFP's SNR_t advantages were no match against the generality and convenience of FT-NMR. Thus SSFP, together with related driven-equilibrium options[25], have remained in the fringes of spectroscopic NMR applications.

Very recently, driven both by curiosity and by promises of increased SNR_t, we revisited SSFP's potential in a number of high resolution spectroscopic applications[20,21]. These spectroscopic studies led to the realization that some of SSFP's main weaknesses –strong offset sensitivity, periodic regions of high and null intensities, repeated folding patterns– may actually contain the seeds for achieving high resolution among inequivalent sites over large bandwidths, as demanded by analytical liquid-state NMR. Based on this we recently proposed an approach to attain high resolution NMR information from SSFP signals, which monitors steady-state responses over a series of offsets $\{\delta_m\}_{0 \le m \le M-1}$ covering the $1/TR$ folding interval, and then exploits the a priori known dependence of a peak's intensity on offset to pinpoint the latter within such interval[22]. In addition, the extreme fold-over associated with SSFP

acquisitions was dealt with by a discrete FT of the short FIDs that were sampled within the inter-pulse intervals TR. Solution-state ^{13}C NMR spectra which compared well with FT-NMR data could then be obtained on simple organic compounds, using this phase-incremented (PI) SSFP approach. Still, given that line shapes in these PI-SSFP spectra did not arise from a FT, their sensitivity and point-spread functions (PSFs) possessed a number of distinctive properties. Most remarkable among them was a dependence of the spectral resolution on the flip-angle α used in the excitation of the spins; this is in marked contrast to resolution in FT-NMR, where line widths are dictated by the duration of the acquired free-induction decay (FID) signals. Indeed, in PI-SSFP NMR arbitrary short acquisition times are no impediment for resolving closely-spaced resonances, as it is the combination of α flip angles being applied and of offsets M being interrogated –but not necessarily to the FID acquisition time given by TR– that govern PI-SSFP's ability to distinguish inequivalent sites. The fact that relatively small αs were then needed to obtain the customary, Hz-sized resolution was then a mixed blessing: on one hand it freed peak intensities from the usual T_1-weighting that affects FT-NMR spectra, but on the other it prevented maximization of the SSFP SNR_t potential –which as illustrated by the | $M_{x,y}$| values presented in Fig. 1, benefits from larger flip angles when considered over an arbitrary range of offsets.

The present study revisits the origins of PI-SSFP's demand for small flip angles to achieve high spectral resolution. It is shown that it is not because of fundamental principles but rather because of instabilities in the data processing, that the resolution of inequivalent peaks in PI-SSFP NMR is complicated when relying on large α flip angles. It is also shown that for common instances, particularly when dealing with sites possessing relatively long longitudinal relaxation times T_1, overcoming these instabilities could lead to substantial SNR_t advantages over the FT-NMR scheme. A generic PI-SSFP formalism coupled to a tailored processing algorithm that, based on such derivations, can deal with large α-angle excitations, is then put forward. The result is a new approach that can provide a spectral sensitivity that matches or exceeds that of 1D FT-NMR experiments based on Ernst-angle excitations, at no compromise in spectral resolution. This is exemplified with a variety of 1D ^{13}C and ^{15}N NMR data. Limitations as well as additional potential extensions and applications of this novel approach to high-resolution NMR, are briefly discussed.
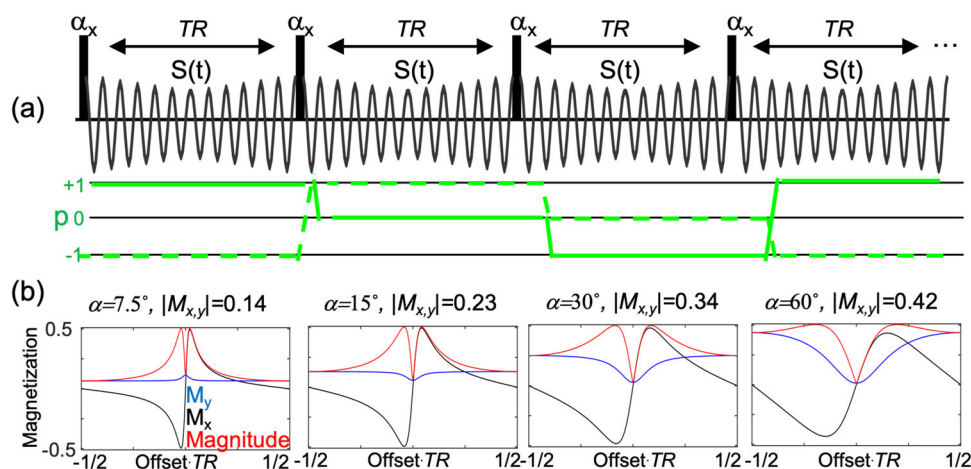

Fig. 1 | Distinctive characteristics of Carr's steady-state free-precession (SSFP) experiment. a SSFP sequence involving a train of pulses α (assumed here applied with constant phase x) spaced by repetition time intervals TR, leading to short time-domain signals S(t). Shown underneath in green is a subset of the coherence transfer pathways p undergone by an isolated spin ensemble under the action of the sequence, illustrating the complex echoing at the top of any given pulse. **b** Steady-state responses S(0) arising at the top of each SSFP pulse as a function of a site's frequency offset, shown for four different flip angles α. Shown as well are the transverse magnetizations M_x (black), M_y (blue) and their magnitude sum | $M_{x,y}$| (red) arising for each flip angle over the full frequency range, and their integrated absolute values. Offsets past ±1/2TR repeat themselves inside this region by repetitive fold-overs.

Theoretical background

A deterministic approach to the 1D PI-SSFP NMR spectral reconstruction

As mentioned, the PI-SSFP proposal to collect high resolution 1D NMR spectra relies on acquiring and processing an array of (signal-averaged) steady-state FIDs of duration TR, as a function of offset. This is best carried out by signal averaging a series of NS scans, where the carrier offset is constant, but the phases of consecutive RF pulses are incremented in steps of $\{\varphi_m = 2\pi m/M\}_{0 \leq m \leq M-1}$ (Fig. 2a). This will provide an array of M FIDs $\{S_m(t)\}_{0 \leq m \leq M-1}$, sampled over times $0 < t < TR$. Assuming for simplicity the presence of a single peak positioned at a frequency f, and given the aforementioned $1/TR$ periodicity of the SSFP signal response S on f, it is possible to describe the ensuing M steady-state FIDs at times $t = 0$ (e.g., immediately after each pulse) as the discrete Fourier series[23,24]

$$S_m(0) = S(0, 2\pi f \cdot TR + \varphi_m)$$
$$= I(f) \cdot \sum_{k=-\infty}^{\infty} A_k \exp(ik\varphi_m) \cdot \exp(ik2\pi f TR), m = 0 \ldots M-1. \quad (1)$$

where $I(f)$ is the spectral intensity of the peak at frequency f. The A_k in Eq. [1] are discrete Fourier coefficients reflecting the multiple transfer pathways depicted in Fig. 1, that can be calculated analytically and whose amplitude decays to zero as $|k|$ increases[23,24]. These coefficients depend on the flip-angle α, on $E_2 = \exp(-TR/T_2)$ and, more weakly, on $E_1 = \exp(-TR/T_1)$; importantly, the larger the flip-angle α or the shorter the T_2, the faster the A_k will decay to zero with $|k|$. We have recently shown[22] that knowledge of these A_k coefficients –whether from

analytical or numerical sources– can allow one to find from the $\{S_m(0)\}_{0 \leq m \leq M-1}$ set, the spectral amplitude $I(f)$ that, after multiple potential foldings within the $\pm 1/2TR$ interval, will characterize a peak of frequency f. Assuming for the sake of simplicity that the frequency being searched for has not folded over, i.e., that $-\frac{1}{2TR} \leq f \leq +\frac{1}{2TR}$, we proposed recreating the NMR spectrum within such range using a linear combination of the $S_m(0)$ signals. Denoting this linear combination as $F(f)$ and the a priori unknown coefficients that will be involved in it as $\{\beta_m\}_{0 \leq m \leq M-1}$, we define the linear combination as

$$F(f) \triangleq \sum_{m=0}^{M-1} \beta_m S_m(0) = \sum_{k=-\infty}^{\infty} \sum_{m=0}^{M-1} A_k \exp(ik\varphi_m) \cdot \beta_m \cdot \exp(ik\,2\pi f\,TR) \quad (2)$$

Achieving high spectral selectivity means that this linear combination function should mimic as closely as possible a discrete band-pass filter, whose line shape will define the "peaks". Based on filter response theory, this filter can be written as

$$R(f) = \sum_{k=-N/2}^{\frac{N}{2}-1} C_k \cdot \exp(ik\,2\pi f\,TR) \quad (3)$$

where the $\{C_k\}_{-N/2 \leq k \leq N/2-1}$ coefficients can be calculated based on a desired response (e.g., using the Finite Impulse Response script in Matlab's signal processing toolbox[25]). Finding the linear combination that makes $F(f)$ as close as possible to $R(f)$ then demands solving a series
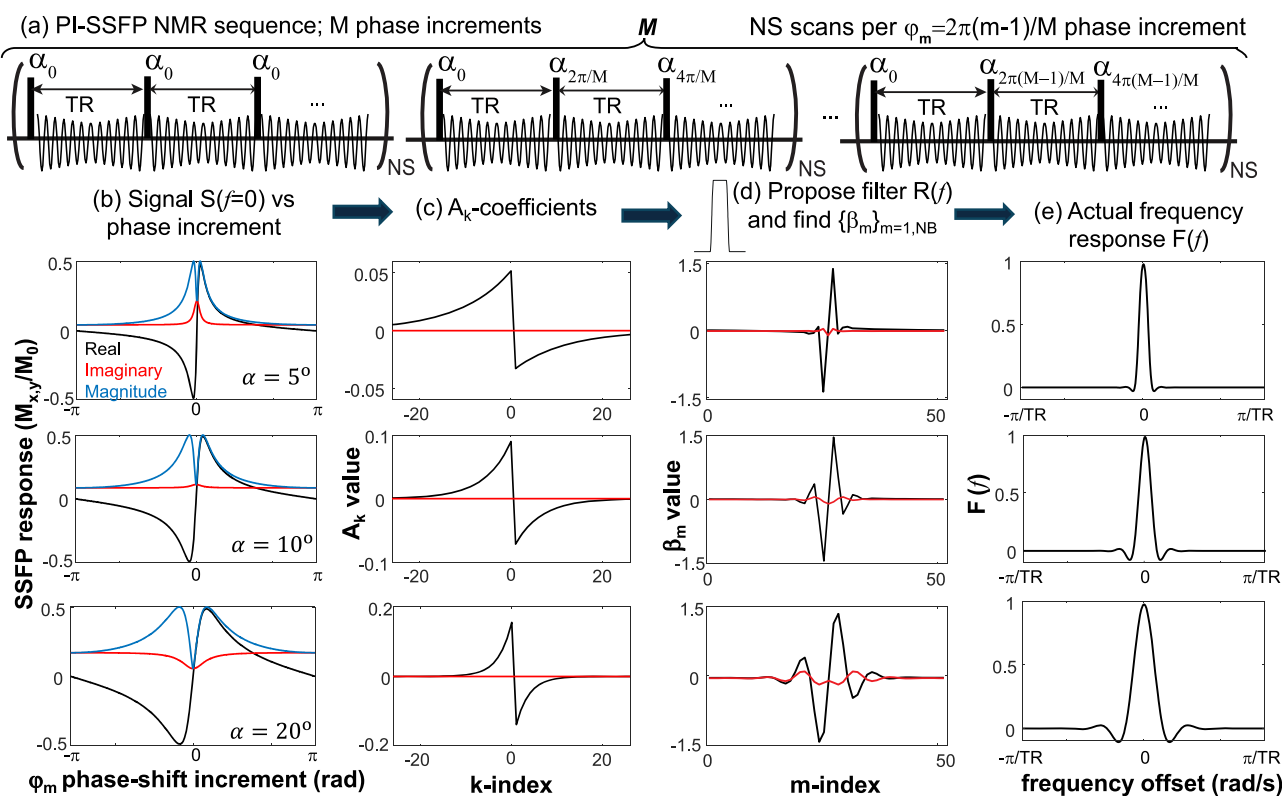

Fig. 2 | Phase-incremented (PI) SSFP approach to high-resolution NMR. a Pulse sequence involving a train of NS signal-averaged scans excited by pulses of flip-angle α spaced by a repetition time TR, and relative phases φ_m incremented as shown over M uninterrupted experiments. **b** Single-site SSFP response vs relative phase increment φ_m for different flip angles α, assuming $f = 0$, $T_1 = 5$ s, $T_2 = 2$ s, and constant (zero) receiver phase. A similar response would arise from pulses with a constant phase as a function of the site's offset. **c** Fourier coefficients $\{A_k\}$ derived

from Eq. [1], describing the SSFP response in (**b**); notice their rapid drop with increasing α. **d** β-coefficients derived from a least-square solution of $L \cdot \beta = C$, needed to recapitulate the illustrated filter centered at zero. **e** Actual frequency response resulting from applying the $\{\beta_m\}$-coefficients on $M = 50$ PI-SSFP experiments upon using $NB = M/2$ frequency bands, evidencing a deteriorating resolution with increasing flip-angle.
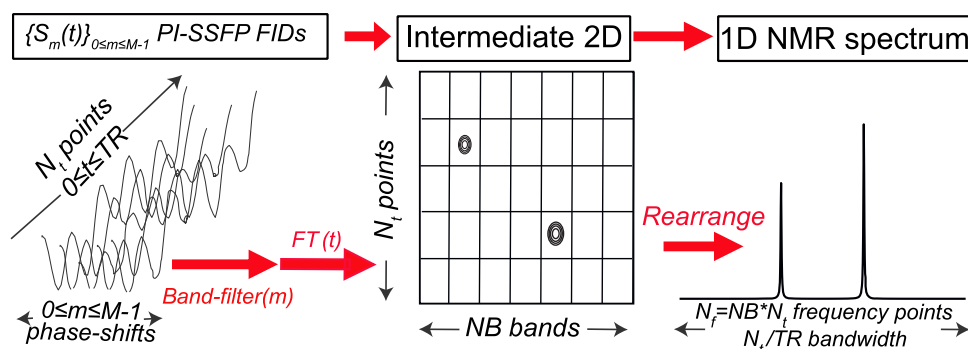
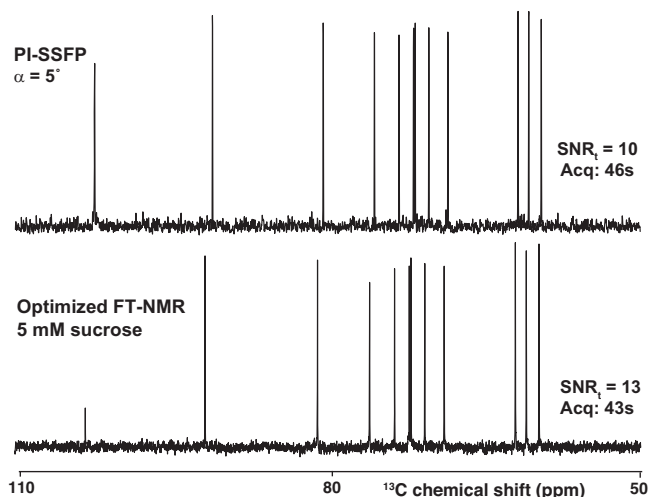**Fig. 3 | Processing PI-SSFP NMR data into high-resolution 1D NMR by band-filtering/Fourier-transform (FT).**

Fig. 4 | {¹H}¹³C NMR spectra of 5 mM sucrose in D₂O recorded (as throughout this paper) at 14.1 T using the indicated overall acquisition times. FT-NMR data was recorded using ≈50° excitation pulses, 0.6 sec acquisition times and no recovery delay (Ernst angle acquisition conditions for a $T_1 \approx 1.5$ sec). PI-SSFP used NS = 200 scans, TR = 30 ms and M = 12. Shown for each experiment is the SNR_t for the strongest peak in the spectrum vs noise from the (peakless) 110-140 ppm range.

of linear equations

$$C_k \approx A_k \sum_{m=0}^{M-1} \beta_m \cdot \exp(ik\varphi_m), k = -\frac{N}{2} \ldots \frac{N}{2} - 1 \quad (4)$$

Suitable solutions $\{\beta_m\}_{0 \leq m \leq M-1}$ of these equations will generate a narrow filter with a targeted width of *1/(TR·NB)* −NB being the total number of bands (peaks) to be resolved within ±1/2TR. Eq. [4] can also be written in matrix form as

$$C \approx L \cdot \beta \quad (5)$$

where **C** is a N-by−1 vector containing the $\{C_k\}_{-N/2 \leq k \leq N/2-1}$ coefficients, **β** is an M-by-1 vector with the $\{\beta_m\}_{0 \leq m \leq M-1}$, and **L** is a N-by-M matrix whose *k,m*-element is

$$L_{k,m} = A_k \exp(ik\varphi_m). \quad (6)$$

The **β**-coefficients needed to define the intensity of a peak at frequency *f* could then be found by minimizing the norm $||C - L\beta||_2^2$ using the Moore-Penrose inverse matrix $\beta = (L^\dagger L)^{-1} L^\dagger C$, where $L^\dagger$ is *L*'s conjugate transpose.

Figure 2 clarifies further these arguments, by describing how this proposal to high resolution NMR (sequence in Fig. 2a) finds a "peak

intensity" at *f* = 0. Illustrated in Fig. 2b is the SSFP response vs phase increment for this site at zero chemical shift, for the array of phase-increments used by the sequence and as a function of increasing flip angles α. Notice that the overall signal magnitude increases steadily with α, but −as adumbrated by the plots in Fig. 1− the offset (i.e., the φ_m) dependence of the SSFP response also "flattens", and thereby loses frequency discrimination insight. This is reflected by the $\{A_k\}$ coefficients (Fig. 2c), which increase in intensity but decay in *k*-span for increasing flip-angles. The ensuing loss in spectral information is also reflected in the $\{\beta_m\}$ set derived from solving Eq. [5], which manages to reconstruct the proposed frequency response with a few central *m*-values when α is small, but calls for large, widely oscillating contributions as most $\{A_k\}$ become zero for large flip angles (Fig. 2d). This reflects an ill-conditioning of the aforementioned **L**-matrix, and ends up leading to peak shapes that only for smaller α's, reflect the narrow filter that was originally designed (Fig. 2e). In other words, in this PI-SSFP-based approach to high-resolution NMR, it is not only signal intensity but also spectral resolution that will be controlled by the excitation pulses.

The **β**-coefficients (Fig. 2d) can be used recursively to interrogate other contributions *I(f)* even if *f* ≠ 0, and thereby to introduce spectral resolution within the ±1/2TR interval. In general *NB* spectral bands will thus become resolvable within this interval; assuming α has been chosen small enough to provide enough $A_k \neq 0$ coefficients, NB will then be dictated by the number *M* of phase increments used in the experiment; in our processing pipeline, we usually set *NB* = M/2. This **β**-based treatment, however, cannot address SSFP's folding problem; therefore, peaks separated by multiples of 1/*TR* (usually tens or hundreds Hz) will end up falling on the same $-\frac{NB}{2} \leq j < \frac{NB}{2} - 1$ band, and their precise resonance positions will remain unknown. As explained in ref. 22 it is possible to endow the SSFP signal in Eq. [1] with a suitably large window that unfolds this information by sampling not just $S_m(0)$, but numerous N_t points within each $0 \leq t \leq TR$ period. Performing discrete FTs on these short $S_m(t)$ FIDs will yield spectra with an overall bandwidth of $\approx 2\pi N_t/TR$, with each data point *p* separated by a frequency increment $\approx 2\pi/TR$ (in angular frequency units). As detailed in Fig. 3, adding onto this FT the phase-incremented filtering procedure described in Fig. 2, can then dissect each of these spectral elements into NB finer bands. Although conceptually simple this reconstruction requires addressing subtle but important issues associated with spectrometer deadtimes and band-dependent offsets, which if left unaddressed lead to spectral artifacts and phase distortions in the resulting peaks. With all these problems being deterministically addressed (ref. 22), Fig. 4 compares the performance of the resulting PI-SSFP approach vs FT-NMR ¹³C results, for a 5 mM sucrose sample in D₂O. For simplicity the Figure, as all data presented in this paper, centers on nuclear Overhauser effect (NOE) enhanced, ¹H-decoupled solution-state acquisitions[4,5]. As can be appreciated the resolution and SNR_t of both methods are comparable, raising the question of what

would then be the advantage of having an SSFP-based approach that, while capable and based on its own processing pipeline, performs similarly as FT-based methods. We turn next to address this question, by describing under which conditions will PI-SSFP exceed FT-NMR's SNR_t performance.

On the demands needed by PI-SSFP to overcome FT-NMR's SNR_t at a given spectral resolution

The reason why the prototypical PI-SSFP spectrum in Fig. 4 does not evidence SNR_t gains over its FT-NMR counterpart, derives from the relatively small flip-angle used in this acquisition. These small α-values were dictated by our search for a stable solution of the $L \cdot \beta \approx C$ system of equations, needed in turn by our desire to obtain spectral linewidths in the 1–2 Hz range. On the other hand, as illustrated in Fig. 1, the overall SNR_t averaged over the $\pm1/2TR$ interval for cases such as this one, where T_1 and T_2 times are relatively similar and peaks would be more-or-less randomly spread, would benefit substantially if larger flip angles were to be employed. To explore further the interplay between sensitivity and resolution in SSFP experiments, Fig. 5 assumes for simplicity that resonances are uniformly distributed over $\pm1/2TR$ (resonances outside such interval would anyhow fold over into it) and compares the averaged signal intensity afforded by SSFP acquisitions carried out as a function of flip angle, vs Ernst-angle-optimized FT-NMR. For all cases a prototypical 2 Hz resolution was assumed; this will dictate the minimal number of bands NB needed in the PI-SSFP acquisitions (disregarding for the moment the flip-angle influence on spectral resolution), and the duration of the FID (assumed equal to the recycle delay) for the FT-NMR case. As in our experience neither experiments nor simulations show a dependence of PI-SSFP's SNR_t on TR (shorter TR means more phase increments are needed to finely cover the $\pm1/TR$ bandwidth but also more scans can be packed per unit time) we also assumed that TRs matched –when multiplied by the number of scans and of phase increments– the overall acquisition duration of the FT-NMR FID. Given that spectral widths can also be chosen arbitrarily in both experiments by controlling the dwell times, this in turn allowed us to equalize both the overall durations of the PI-SSFP and FT NMR time-domains, and the bandwidths of the acquisitions; as a result, the noise that would affect both experiments would also be equalized. Based on these assumptions, it is solely the overall transverse magnetizations elicited from the spins, that will define the relative SNR_t performances of the FT-NMR and PI-SSFP experiments. Figure 5 plots the relative merits that, under these assumptions, the two experiments will exhibit for T_1 and T_2 values often encountered in analytical ^{13}C NMR, as a function of the SSFP flip-angle employed. These plots show that in most cases, but particularly for the longer T_2 values favoring SSFP's $T_1 = T_2$ maximum signal intensity conditions, the SSFP experiment can exceed FT-NMR's sensitivity –even when considering the SSFP "dark" bands. However, to achieve such superior SNR_t, relatively large (≥15°) flip angles will have to be used. And hence

the dichotomy of the PI-SSFP approach as described so far: To deliver high resolution the aforementioned **L** matrix needs to be well conditioned and for this the SSFP acquisition needs to be performed using relatively small (≈5-10°) flip angles; on the other hand, in order to maximize its sensitivity potential, SSFP data should be collected using relatively large flip angles.

Achieving PI-SSFP's SNR_t potential: Increasing flip-angles without compromising spectral resolution

To address these conflicting demands and realize PI-SSFP's SNR_t potential without compromising on the approach's spectral resolution, we revisit the PI-SSFP experiment and discuss a processing alternative that departs from the one which led to the spectrum in Fig. 3. Still, in the same way as the approach used in Fig. 3 had to solve an $L \cdot \beta = C$ linear system of equations –and in analogy with the linear $Ax = b$ equation underlying FT-NMR, where A is an inverse FT matrix, x the spectrum being sought and b the collected FID– also the new approach to be here discussed will require solving a system of linear equations. This is because in PI-SSFP, as in FT-NMR, a linear relation links the data being collected, with the spectrum being sought. In the FT-NMR case, inverting the system of equations linking the collected FID with the sought spectrum can be done readily, thanks to the ideal conditioning of the discrete FT matrix. In PI-SSFP experiments collected as a function of phase increment m and acquisition time t there will also be a linear relation between the data and the high-resolution NMR spectrum. The question is what are the equations relating the two, and how can a stable inversion of these equations be performed, even when using the large flip angles that maximize SSFP's SNR_t.

To derive the linear relation in question, we rewrite the short array of FIDs collected in PI-SSFP experiments as a function of $0 \le m \le M-1$ phase increments (the $S_m(t)$ in Fig. 3), as a frequency-dependent construct $S_f(t, m)$. For this we start with the $t = 0$ expression in Eq. [1], and describe the full array of collected FIDs as

$$S_m(t) = \sum_f S_m(0) \exp(-i2\pi f t)$$

$$= \sum_f I(f) \exp(-i2\pi f t) \cdot \sum_{k=-\infty}^{\infty} A_k \exp(ik\varphi_m) \cdot \exp(ik2\pi f TR)$$

$$(7)$$

where the final spectrum being sought is given by the sum of all $I(f)$ amplitudes, $I = \sum_f I(f)$. Given that the times t within each FID are discretely sampled over N_t equally spaced instants, and assuming as is customary in NMR that the frequencies f will be discretized over N_f different values, it is possible to rewrite Eq. [7] in matrix form as

$$\underbrace{S_f(t,m)}_{N_t \times M} = \underbrace{F(t,f)}_{N_t \times N_f} \cdot \underbrace{I(f)}_{N_f \times N_f} \cdot \underbrace{D(f,m)}_{N_f \times M} \qquad (8)$$
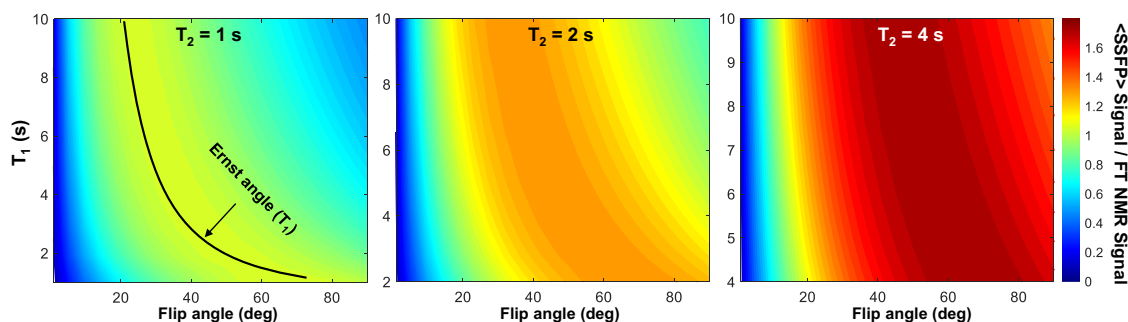

Fig. 5 | Ratio between weighted SSFP signal intensities integrated over the ±1/2TR interval vs frequency-independent FT-NMR signal intensities as a function of the SSFP flip angle α, for a range of T_1, T_2 values. Shown for completion is the Ernst angle used for various T_1s (left), assuming in all cases a 2 Hz spectral resolution (see text for further details).

In this Equation –which for completion shows the dimensions (rows × columns) of each of the constructs– $\boldsymbol{S}_f(t,m)$ still represents the $S_m(t)$ set of PI-SSFP FIDs, stressing now that they will be influenced by the frequency-domain peak intensities as well. $\boldsymbol{F}(t,f) = \exp(-i2\pi ft)$ is a Fourier function, discretized into a matrix among the N_t-values of time $0 < t < TR$ that were sampled and among the N_f discrete frequencies $\{f_l\}_{0 \le l \le N_f - 1}$ over which the spectrum will be reconstructed. $\boldsymbol{I}(f) = \sum_l I(f_l)$ is a square $N_f \times N_f$ matrix whose only non-zero elements lie along the diagonal, and contain the high-resolution spectral information being sought, as given by an intensity I for each frequency f_l (i.e., I is also as $N_f \times N_f$ matrix). Finally, $\boldsymbol{D}(f,m) = \sum_k A_k \exp(i2\pi m \cdot k/M) \cdot \exp(i2\pi kf\, TR)$ is the SSFP matrix in Eq. [1], with f once again discretized over N_f elements and m denoting each phase-incremented acquisition.

As follows from these equations, and as further elaborated in the Supplementary Information, it can be shown from Eq. [8] that for each frequency f_l being interrogated, there will be a linear relationship linking the PI-SSFP signals measured, and the spectral intensity $I(f)$ being sought: $\boldsymbol{S}_l(t,m) = I(f_l) \cdot (\boldsymbol{F} \cdot \boldsymbol{D})_l$, where $(\boldsymbol{F} \cdot \boldsymbol{D})_l = \boldsymbol{G}_l$ is an $N_t \times M$ matrix resulting from calculating the $\boldsymbol{F} \cdot \boldsymbol{I} \cdot \boldsymbol{D}$ product, assuming that in $\boldsymbol{I}$ only a single line at frequency f_l was present. Expanding then each $\boldsymbol{S}_l$, $\boldsymbol{G}_l$ matrix into single vectors of length $N_t{\cdot}M$, we end up having $\boldsymbol{S}_l = I(f_l) \cdot \boldsymbol{G}_l$, where both $\boldsymbol{S}_l$ and $\boldsymbol{G}_l$ are vectors with $N_t{\cdot}M$ elements. Repeating this argument for each frequency $\{f_l\}_{0 \le l \le N_f - 1}$, will transform $\boldsymbol{G}$ into a "supermatrix" $\boldsymbol{\Xi}$ of dimensions $N_t{\cdot}M \times N_f$, that is related to the spectral vector as

$$\boldsymbol{S}_l = \boldsymbol{\Xi} \cdot \boldsymbol{I}(f_l). \tag{9}$$

Here $\boldsymbol{I}(f_l)$ is an $N_f \times 1$ vector whose elements are zero for all frequencies except f_l, where it then takes the value $I(f_l)$. (This transitioning of matrices into vectors that are then lined up into new "supermatrices", is akin the transformation of spin operators –matrices in Hilbert space– into vectors, that are then subject to the action of "supermatrices" like Redfield's relaxation superoperator). Hence, the sum of these vectors for all f_l, $\mathcal{I}(f) = \sum_{l=0}^{N_f - 1} \mathcal{I}_l(f)$, is the spectrum being sought. This sum can also be applied directly onto Eq. [9], leading to

$$\sum_{l=0}^{N_f - 1} \boldsymbol{S}_l = \boldsymbol{\Sigma} = \boldsymbol{\Xi} \cdot \sum_{l=0}^{N_f - 1} \boldsymbol{I}(f_l) = \boldsymbol{\Xi} \cdot \boldsymbol{I}(f). \tag{10}$$

The $\boldsymbol{\Xi} \cdot \boldsymbol{I}(f) = \boldsymbol{\Sigma}$ form in Eq. [10] highlights the linear, $\boldsymbol{A}x = b$–type relation linking the measured PI-SSFP information in $\boldsymbol{\Sigma}$, with the spectrum residing in $\boldsymbol{I}(f)$ via a transform matrix $\boldsymbol{\Xi}$. As done above for the $\boldsymbol{\beta}$-coefficients, one could in principle solve this problem in a frequency-by-frequency basis, via a least-square or pseudo-inverse solution. However, because of the considerations discussed above in connection to Fig. 2, the $\boldsymbol{G}_l$ matrices will be ill-posed for inversion when the SSFP data are collected utilizing large flip-angle pulses. To solve this complication, we propose aiding the process of resolving the $\boldsymbol{\Xi} \cdot \boldsymbol{I}(f) = \boldsymbol{\Sigma}$ equation with the help of regularization. In particular, we replace the solutions derived from the above-mentioned $\boldsymbol{\beta}$-coefficients, with a least absolute shrinkage and selection operator (LASSO) regression analysis[26–28], which is particularly efficient when the solution being sought is relatively sparse –as will be the case when dealing with a high resolution NMR spectrum[29,30]. In this case, LASSO will search for the $\mathcal{I}(f)$ "spectrum" that minimizes

$$\mathcal{L} = \min_{\mathcal{I} \in \mathbb{C}^{N_f}} \left\{ \frac{1}{2} \|\boldsymbol{\Xi} \cdot \mathcal{I} - \boldsymbol{\Sigma}\|_2^2 + \lambda \|\mathcal{I}\|_1 \right\}, \tag{11}$$

where $\| \|_{1,2}$ stand for the first and second norm respectively, and $\lambda > 0$ is a regularization parameter promoting a solution that conforms to the general sparsity of high-resolution NMR spectra. (This adaptation of a forward-fitting model to the PI-SSFP acquisition seeking to minimize the spectral L1 norm has parallels with soft thresholding and maximum entropy approaches used in NMR and MRI[29–31]. While in MRI a sparsifying operation –e.g., a wavelet transformation– is needed to make the solution being sought sparse, NMR spectra of the kind being here considered do not need this extra step. See Supplementary Information for further details). In the present study, the FISTA algorithm, which is an implementation known to solve LASSO problems efficiently, was adopted for calculating the $\mathcal{I}(f)$ spectra.

Figure 6 presents simulations incorporating fixed noise levels and PI-SSFP data collected with a variety of flip angles, comparing the processing capabilities of the $\boldsymbol{\beta}$-filter-based proposition, with the L1 (first-norm) regularized LASSO reconstruction described in Eq. [11]. For each flip angle the signals being subject to these two processing pipelines are the same, and in all cases consisted of four peaks of relative intensities 1:0.4:0.1:0.7, affected by identical, α-independent levels of time-domain noise. These examples illustrate how the LASSO approach can deal with PI-SSFP data recorded for larger flip angles, retaining peak linewidths constant and improving the peak's intensities as the signal arising from increased flip-angles becomes larger. This is particularly evident for the peak with relative intensity of 0.1 placed at 1.0 kHz, which clearly emerges from the noise at higher αs. By contrast, PI-SSFP data processed using the $\boldsymbol{\beta}$-based coefficients leads to broadened peaks when processing the larger-flip-angle FIDs, and thereby to minor decreases in the SNR despite the larger signals emitted by the spins at larger αs.

The fact that the LASSO-based processing largely decouples peak line widths from flip-angles, raises in turn the issue of what will be the spectral resolution achievable by PI-SSFP data processed by this pipeline. To solve a problem like the one in Eq. [10] solely based on a least-square fit, the number of rows in $\boldsymbol{\Xi}$ should exceed the number of columns in the matrix; in other words, $N_t{\cdot}M \ge N_f$. As for a given TR the spectral bandwidth will be $1/\Delta t$, where $\Delta t \approx TR/N_t$, the minimal frequency resolution that a least-square approach should be able to resolve will be $\Delta f \ge \frac{1}{TR \cdot M}$. When implementing the β-based reconstruction our experience was that quality spectra could be obtained upon setting $\Delta f = \frac{2}{TR \cdot M}$, provided that relatively small (≤10°) flip-angles were employed[22]. By contrast, and, thanks to the introduction of the regularization term in Eq. [11], we find that the $N_f = N_t{\cdot}M$ condition is often well tolerated even when using α ≈ 20–25°; for the results presented below, spectral resolution was usually set like that upon reconstruction: $\Delta f = \frac{1}{TR \cdot M}$. In principle, however, $N_f > N_t{\cdot}M$ also works in noiseless conditions. Notice as well that while all the elements involved in this reconstruction are complex, peaks in the ensuing $\boldsymbol{I}(f)$ spectrum will have no dispersive components. Hence, and although imaginary parts of these spectra are usually close to zero, the data below are plotted in magnitude mode.

Results

Figure 7 presents an illustrative set of results, collected on a caffeine sample. These results include an FT-NMR experiment collected in ca. 180 s under optimized Ernst-angle conditions (a), and a PI-SSFP acquisition collected in a similar time using 20° flip-angle pulses and 12 phase increments. This acquisition was in turn processed using the $\boldsymbol{\beta}$-based approach introduced in ref. 22 / Fig. 3b, and the new regularized reconstruction summarized in Eq. [9] (c). Highlighted on the colored insets, are the line shape improvements brought about by the new processing alternative. Also shown in the Figure is ancillary information including the peak assignment (center), the T_1 times measured for each site (top), and the ratio between the SNR_t obtained for each peak in the FT-NMR and in the regularized PI-SSFP spectra (bottom). The actual SNR_t enhancements are not important per se in absolute terms, as noise and sensitivity in regularized reconstructions is a complex subject requiring statistical analyses for elucidation. Still,
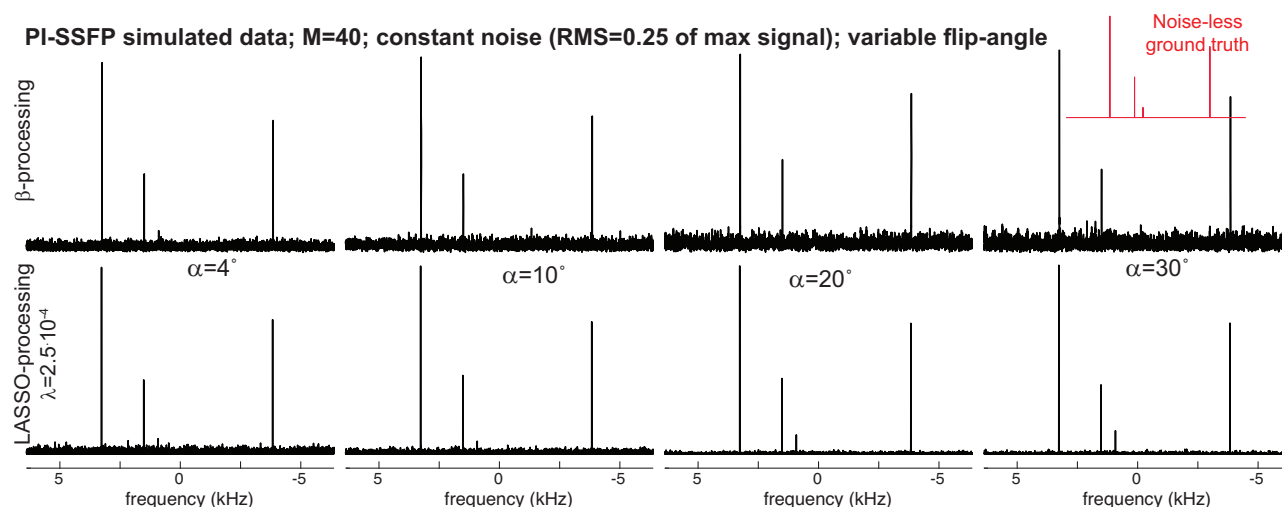
Fig. 6 | Synthetic NMR spectra reconstructed for four uncoupled sites with relative intensities 1:0.4:0.1:0.7 positioned at 3.5, 1.6, 1.0 and -4.05 kHz, assumed subject to PI-SSFP experiments with different flip-angles α. Additional common parameters of all "experiments" included TR = 20 ms, M = 40 phase increments, 13.5 kHz sampling rates, 2 Hz digital resolutions, instantaneous (δ) pulses, identical relaxation times $T_1 = 5$ s, $T_2 = 2$ s, and a constant (α-independent) noise level created by a random number generator with an RMS amplitude amounting to 25 % of the maximum single-site longitudinal magnetization (the peak at 3,5 kHz). Notice the slight SNR drop that data "acquired" for increasing α shows when processed based on the β-coefficients, despite the increase signals emitted as flip-angles increase (Fig. 1). We ascribe this to a broadening of the β-derived filter functions, which is absent in the regularized version that keeps all peaks at similar half widths regardless of the flip angle used in the PI-SSFP acquisition. No such penalty affects the regularized reconstruction introduced in this work.

notice how when dealing with non-protonated sites with relatively long T_1s, the PI-SSFP sensitivity advantage is clearly seen. Notice as well how a departure of the $T_2/T_1 \approx 1$ ratio matters in these sensitivity gains: for instance, ^{13}Cs that are bonded to multiple ^{14}N nuclei and have long T_1s but for which $T_2/T_1 \ll 1$, exhibit less impressive sensitivity gains –as reported in other SSFP studies[32]– than other quaternary carbon counterparts.

Figures 8, 9 highlight the capability of the new processing procedure to deliver excellent peak shapes over arbitrary bandwidths, while sometimes exhibiting clear SNR_t advantages over FT-NMR. Notice how PI-SSFP's sensitivity will match that of FT-NMR for most of the peaks, but make sites with longer T_1s –whose signals are sometimes buried in the FT-NMR spectral noise– appear with good sensitivity within similar acquisition times. Notice as well that while relying on relatively large flip angles, an improved spectral resolution characterizes the LASSO reconstructions over the **β**-based counterparts. The advantages seem particularly large in the case of the non-protonated amines in Fig. 9, which since devoid of ^{1}H NOEs and given ^{15}N's low natural abundance, present a significant challenge to FT-NMR. The long T_1s of these non-protonated sites further compounds this problem; although these were not evaluated for all the assayed compounds, T_1 was found to be on the order of 40 s for pyridine's ^{15}N, and based on this value the excitation pulses used in FT-NMR acquisition were set. Judging by the observed peak intensities, it appears that for some of the remaining compounds examined the ^{15}N T_1s were even longer; in all these cases, the advantages of PI-SSFP were most evident.

Discussion
The present study sought to endow the PI-SSFP approach to high-resolution NMR, with the sensitivity advantages known to characterize SSFP for $T_1 \approx T_2$ conditions. These sensitivity advantages will come into play foremost when seeking resolution and having to deal with sites with long T_1s: FT-NMR resolution considerations will then demand the use of relatively long acquisition times TR, while Ernst-angle constraints will then require small flip-angles $\alpha_E = \cos^{-1}(e^{-TR/T_1})$ to maximize spectral SNR_t. By contrast no such long-TR demands will affect PI-SSFP, whose resolution is given by the flip-angle and the number of

employed phase increments. However, to make full use of the ensuing competitiveness, one still needs to have the option of collecting the PI-SSFP experiments over a range of flip angles. In particular, when $T_1 \approx T_2$, optimal SSFP SNR_t conditions will demand working with flip-angles in the ≥40° range; according to our previously proposed implementation, this would bring about an ill-conditioning of the data processing, and lead to a broadening in the point-spread functions characterizing the peaks. By casting the problem in a different, $\mathbf{A}x = b$ fashion susceptible to a least-square regularized inversion, this study lifts such limitation. Regularization then enabled us to work at high flip-angles without compromising the spectral resolution; notice, however, that whenever dealing with very long T_1s –including in several of the sites in the compounds here assayed– the $T_2 < T_1$ condition will still require relatively small flip angles for an optimal SNR_t.

The demonstration that PI-SSFP signals and 1D NMR spectra are linearly related to one another (Eqs. [9], [10]), endows the PI-SSFP experiment with a few processing alternatives. The present study adopted one of them, based on an L1-regularized procedure. Other regularization options were also tested, but LASSO's FISTA-based implementation provided the most satisfying results in terms of line shapes and robustness. The present study concentrated on principles and analyses pertaining to isolated ensembles like those found in ^{1}H-decoupled ^{13}C or ^{15}N NMR at natural abundance; preliminary studies show that the same analyses can be extended to systems involving J-coupled ensembles under high field condition –as long as relaxation times are long vs TR, and SSFP does not depart the small tip-angle approximation.

Unfortunately, the use of LASSO-regularized least-square procedures to reconstruct a spectrum, is also associated to drawbacks and challenges. In terms of drawbacks, the most evident one is paid in terms of computation: whereas processing an 8 kHz spectrum with a 1.3 Hz resolution takes ca. 20 sec on a 16-core i7 desktop computer when implemented by the iterative LASSO approach, the same spectrum was processed in 0.5 sec by the non-iterative β-coefficient formalism (which then lead to ≥3 Hz spectral resolutions). Associated more with the appearance that one expects from an NMR spectrum than with the essence of the information, is the positive-only nature
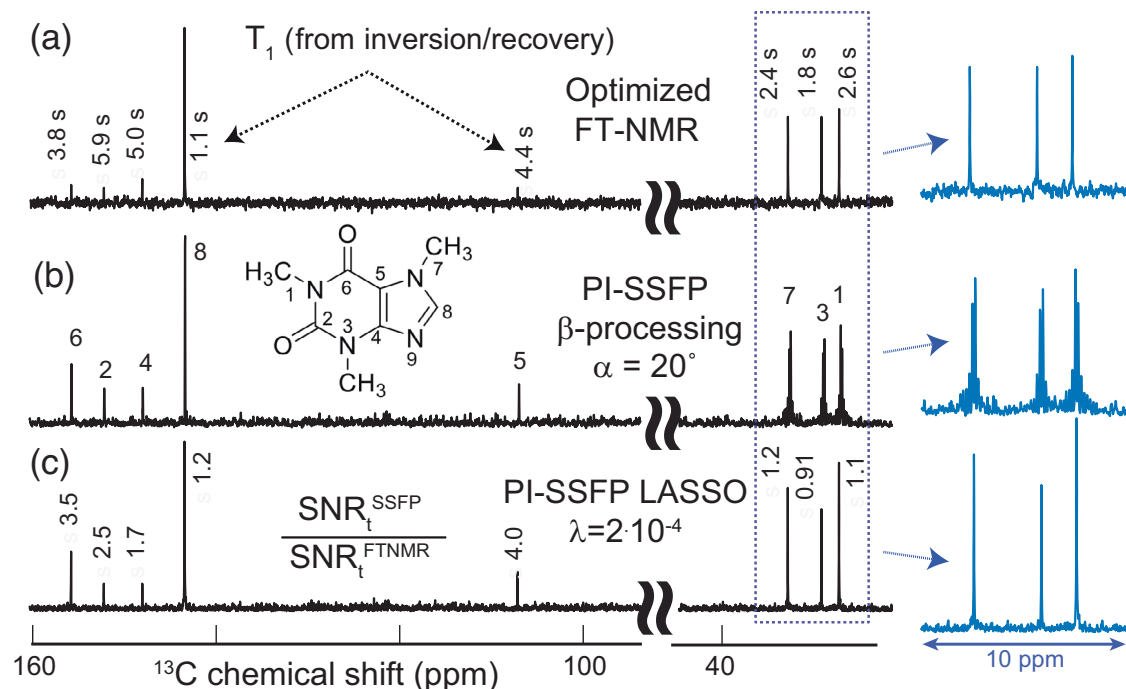
Fig. 7 | {¹H}¹³C NMR spectra of 50 mM caffeine in D₂O recorded using optimized FT-NMR and PI-SSFP. a FT-NMR data recorded with a 50° excitation, 0.65 s acquisition, no extra delays, 2 Hz line broadening. **b, c** PI-SSFP data recorded with TR = 30 ms, M = 12, α=20°, processing as described. Shown as well are T_1 values measured for individual peaks (**a**), site assignments (**b**), and peak-by-peak ratios between the SNR$_t$s of the LASSO-processed PI-SSFP and the FT-NMR (**c**). Notice how slowly relaxing sites benefit the most SNR$_t$-wise from PI-SSFP, and how minor artifacts in PI-SSFP data processed based on the β-coefficients disappear in the LASSO pipeline. All data were collected in ca. 180 s. Empty spectral regions were cropped away for clarity.
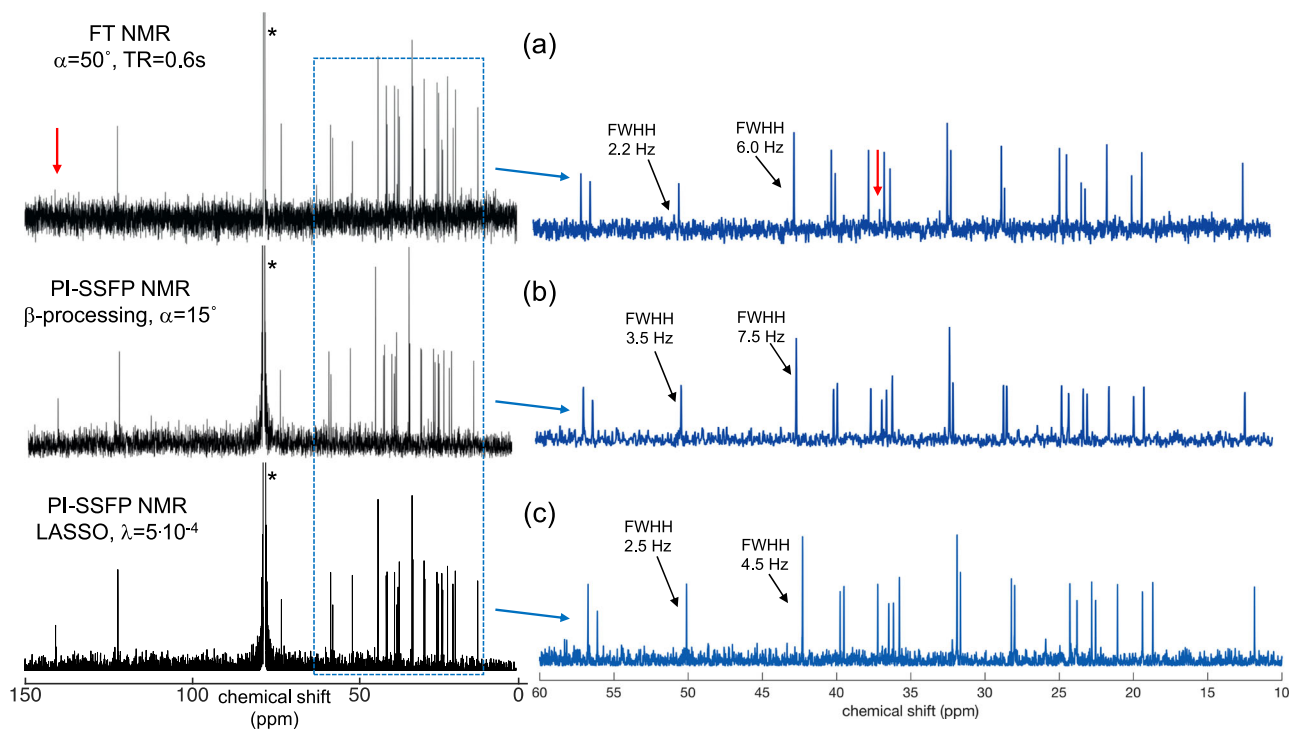
Fig. 8 | Idem as in Fig. 7, but for a 7 mM cholesterol solution in CDCl₃. FT-NMR (**a**) and PI-SSFP (**b, c**) sets were collected in 40 s; traces in blue show zoom-ins to the 10–60 ppm regions. Listed for each trace are main experimental acquisition conditions; the PI-SSFP data involved M = 12 phase shifts with a TR = 30 ms. Indicated are the full-widths at half-height (FWHH) of representative peaks. Red arrows highlight quaternary carbons C1 and C12 at 141 and 36.5 ppm, possessing longer T_1s that negatively bias sensitivity in conventional FT-NMR but not in the new PI-SSFP experiment. All remaining visible peaks have T_1s ≤ 1s. The cropped solvent peak is indicated by an asterisk.
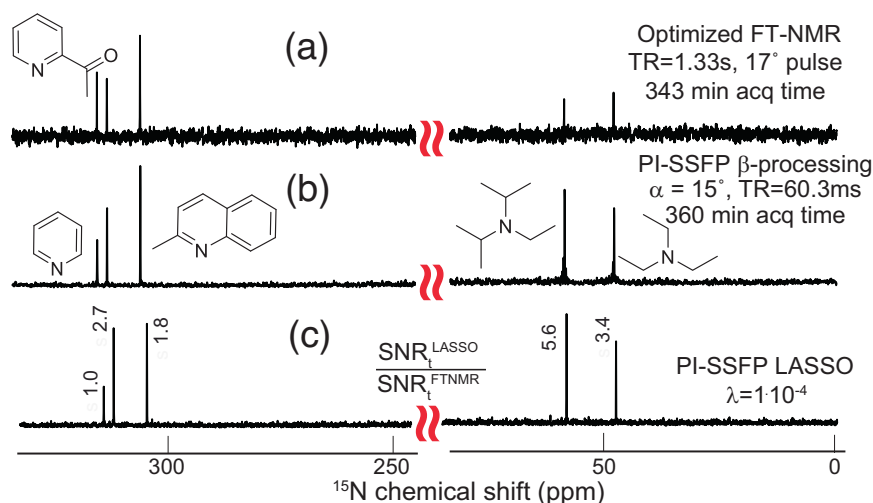
Fig. 9 | [¹H]¹⁵N NMR spectra of equal (50 µL) volumes of the five indicated nitrogenated bases, dissolved in 250 µL of d₆-DMSO. a FT-NMR data processed with a 2 Hz line broadening, yielding line widths ranging between 2.0 and 2.3 Hz. **b**, **c** PI-SSFP data with β-processed linewidths ranging between 4.0 and 4.6 Hz, and LASSO-derived line widths ≈1.9–2.4 Hz. Data were collected in nearly the same acquisition times, leading to the SNR$_t$ ratios between the PI-SSFP LASSO and FT-NMR data indicated next to each peak (the ratios for the β-processed peaks were similar). Empty spectral regions were cropped away for clarity.

of the spectrum that arises from the LASSO iterative fit: both FT-NMR and the non-regularized, least-squares nature of the β-coefficient processing, provide positive and negative spectral intensities that appear more "natural" than LASSO's outcome. An additional complexity associated with this new approach relates to what should be the value chosen for the regularization factor λ. Driven by similar questions arising in the realm of AI, where an extensive literature exists about the effects of such regularization parameters[26–28]. LASSO reconstructions are known to provide reliable solutions of linear sparse problems like that posed by high-resolution NMR –where a spectrum that may span 10^4–10^5 points, will contain only ≈10^2 genuine non-zero frequency elements[33]. In such cases changing lambda will barely affect the intensities of the relevant coefficients, which in 1D NMR correspond to the frequencies where genuine peak intensities are present. Conversely, increasing λ will take the amplitudes of frequencies that do not contribute to the data fitting –i.e., the noise– to zero. From a "cosmetic" point of view this will make LASSO-normalized NMR spectra look as if they are highly dependent on the lambda factor chosen; yet the genuine, peak-relevant information, will be there with faithful intensities and line widths for a relatively large set of λs. Figure 10 illustrates this by comparing spectra emerging upon using different λ-values to perform the LASSO reconstruction on the PI-SSFP ¹⁵N NMR data introduced in Fig. 9. Notice here how, in terms of relative strength, the genuine peaks' relative heights are much less affected than the noise as lambda increases; the AI literature suggests that in such sparse spectral searches, λ values could be increased until ca. $noise_{rms} \cdot \sqrt{\log(peaks)}$ without undue penalties[34]. Notice as well how spectral line widths in the final reconstructions, are virtually independent of the chosen λ. A more complex issue concerns what will be the sensitivity of the LASSO-based reconstruction –in the sense of what is their ability to distinguish a genuine peak out of random noise. This concerns the true measure of the method's sensitivity, and it is a topic still under investigation. Also the ultimate spectral resolution that can be achieved upon invoking regularization, remains to be elucidated. Indeed, when relying on the β-based processing, relatively straightforward relations linked the width of the PI-SSFP point-spread-function to the flip-angle and to the number of phase increments that needed to be collected to distinguish the various $A_k \neq 0$ coefficients. However, upon including a regularization process, spectral resolution can be substantially increased beyond the aforementioned Δf =

$\frac{1}{TR \cdot M}$ limit. The amount of noise will then play an important role on how large can such resolution enhancement be: if the spectral data is sparse (which it usually is) and devoid of noise, as few as $M = 3$ increments may suffice to unravel even complex multiline spectra; basically, as long as MN_t is larger than the number of peaks, the spectrum can be recapitulated with the help of the LASSO regularization. This in turn also highlights the fact that, while we have been performing comparisons against NMR data processed by the usual discrete FT, comparisons against alternative, regularized-based processing approaches might also be relevant. These might make Ernst-angle-based acquisitions more competitive –even if they would likely not overcome the physics-based insight from Fig. 5, showing that spins in SSFP-based experiments will generate the highest signals per unit time.

Another factor that remains to be unraveled concerns how will T_1 and T_2 times affect the PI-SSFP line shapes. The influence of these times is very well understood in multi-scan FT-NMR: here T_1 will define the signal intensity via the Ernst angle, and T_2 the line width and the optimal matching weighting function to be used. The actual FT inversion relating a FID to a spectrum, however, is independent of these time constants. By contrast, T_1 and T_2 enter in the definition of the Ξ PI-SSFP transformation matrix, meaning that line shapes may become affected if these are unknown or very wrongly assumed. While we have not found significant evidence for such effects in numerical simulations, this is a feature that remains to be further investigated. Another intriguing possibility concerns what will happen if steady-states are not necessarily reached over the PI-SSFP procedure; SSFP experiments have, after all, been extensively used in hyperpolarized NMR imaging, under scenarios where polarizations are rapidly decreasing over the course of the pulsing[35–37]. We hypothesize that even under such cases, suitable processing avenues could still enable the acquisition of high resolution NMR spectra via phase-incremented, rapid-pulsing approaches, by relying on the linear relations and principles described above. Additional ways of exploiting this linearity to retrieve spectra that are not based on regularized reconstruction, can also be devised. These and other aspects of this intriguing new route to high-resolution NMR, will be discussed in upcoming studies.

Methods
All samples investigated in this study were purchased from Sigma/Aldrich and used as received. NMR experiments were performed on a
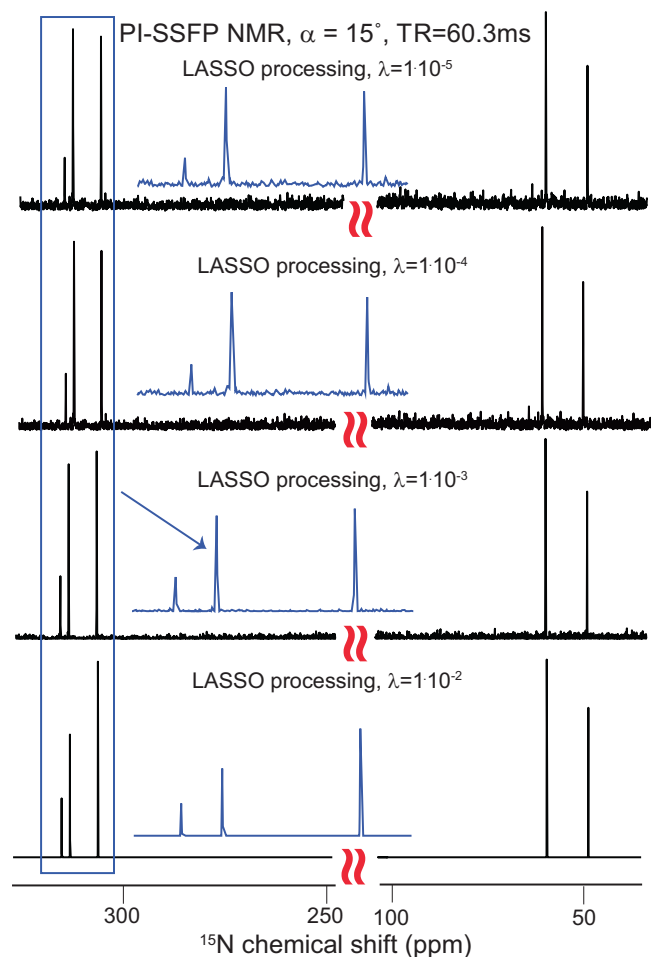
Fig. 10 | Effects of choosing different regularization factors λ on the LASSO-based PI-SSFP data processing. This is exemplified on the {1H}15 N NMR data introduced in Fig. 9. Notice that, in accordance to the literature[33,34], the effect is largely cosmetic: frequency elements devoid of influence are progressively suppressed until becoming null, while spectral elements containing meaningful information (i.e., the peaks) remain mostly untouched in both amplitude and spread (line width). Blue traces are zoomed regions from the indicated peaks; empty regions were cropped away for clarity.

Bruker 600 MHz spectrometer using an AVIII HD console running the Topspin 3.2 software, and equipped with a TCI Prodigy® probe. The SSFP pulse sequence was written on the basis of two nested loops, whereby a train of M α_{φ_m}-FID acquisition sets, possessing flip angles α and having their RF phases serially incremented by $\{\varphi_m = (m - 1) \cdot \Delta\varphi\}_{1 \le m \le M}$, were looped M times while incrementing their Δφ's as $\Delta\varphi_k = (k - 1) \cdot \frac{360°}{M}$. The receiver mode was set to "user defined" in the experiments to minimize complications arising from the machine's digital filtering, and transmitted powers were reduced to 10 W to have a better accuracy in the length of the flip-angles –particularly for small αs. As the inter-pulse delay TR was only a few milliseconds, this was repeated ceaselessly NS times for the sake of signal averaging, and the ensuing signals were coadded. Given the minor changes in the phase shifts Δφ upon going from experiment k to experiment k + 1 coupled to the relatively small angles α used –leading to changes that happen with a relatively high adiabaticity throughout the M acquisitions– no dummy scans were used (although it remains to be seen how closely the steady state was then kept upon changing $\Delta\varphi_k$). Care was taken to minimize the number of points that were lost due to pulse width and receiver deadtime effects. This was done by using relatively large (40-200 kHz) receiver bandwidths, leading to short (≤20 µs) DE deadtimes; these choices did not incur in any

penalties SNR-wise. All experiments used continuous GARP-based heteronuclear 1H decoupling, leading when applicable to NOEs. When reported, relaxation times T1 were measured using an inversion-recovery sequence and fitted using Topspin's relaxation toolbox. SNR was in all cases calculated as the maximum of the signal divided by the standard deviation of the noise; reported SNRt correspond to these SNR values after division by $\sqrt{total\_acquisition\_time}$. PI-SSFP data were processed using Matlab® (The Mathworks Inc.) scripts. SSFP sequences were simulated and processed using Matlab-based codes, considering T1 and T2 relaxation but devoid of couplings effects.

Reporting summary
Further information on research design is available in the Nature Portfolio Reporting Summary linked to this article.

Data availability
The raw PI-SSFP NMR data presented in this study has been deposited and is available as Source Data in https://doi.org/10.34933/d5568eb7-010d-4d75-bc12-064b8c4c5fae. Additional data and simulations described in the present work are available from the authors upon request.

Code availability
A package for implementing the 1H-decoupled 13C/15N high resolution Phase-Incremented Steady State Free Precession NMR experiments described on this study, including the pulse sequence and a processing python script taking the PI-SSFP data and transforming it into a 1D high resolution spectrum using the LASSO (FISTA) algorithm here described, can be found at https://www.weizmann.ac.il/chembiophys/Frydman_group/software (Bruker spectrometers running TopSpin 3.5 only). A basic methanol data sets on which to implement the processing, is also provided.

References
1.   Ernst, R. R., Bodenhausen G., & Wokaun A. *Principles of Nuclear Magnetic Resonance in One and Two Dimensions*, Clarendon, Oxford (1987).
2.   Cavanagh J., Fairbrother W. J., Palmer. A. G., & Skelton N. J. *Protein NMR Spectroscopy: Principles and Practice*, Elsevier (2007).
3.   Levitt, M. H. *Spin dynamics: basics of nuclear magnetic resonance*, Wiley (2010).
4.   Keeler, J. *Understanding NMR Spectroscopy, 2nd Edition*, Wiley (2010).
5.   Claridge,T. D. W. *High-Resolution NMR Techniques in Organic Chemistry: Third Edition*, Elsevier (2016).
6.   Ernst, R. R. & Anderson, W. A. Application of fourier transform spectroscopy to magnetic resonance. *Rev. Sci. Instrum.* **37**, 93–102 (1966).
7.   Kumar, A. & Ernst, R. R. NMR Fourier zeugmatography. *J. Magn. Reson.* **18**, 69 (1975).
8.   Carr, H. Y. Steady-state free precession in nuclear magnetic resonance. *Phys. Rev.* **12**, 1693–1700 (1958).
9.   Freeman, R. & Hill, H. D. W. Phase and intensity anomalies in fourier transform NMR. *J. Magn. Reson.* **4**, 366–383 (1971).
10. Schwenk, A. Steady-state techniques for low sensitivity and slowly relaxing nuclei. *Prog. Nucl. Magn. Reson. Spectrosc.* **17**, 69–140 (1985).
11. Rudakov, T. Some aspects of the effective detection of ammonium nitrate-based explosives by pulsed NQR method. *Appl. Magn. Reson.* **43**, 557–566 (2012).
12. Wolf, T., Jaroszewicz, M. J. & Frydman, L. Steady-state free precession and solid-state NMR. How, when, and why. *J. Phys. Chem. C.* **125**, 1544–1556 (2021).
13. Moraes, T. B. et al. Steady-state free precession sequences for high and low field NMR spectroscopy in solution: Challenges and opportunities. *J. Magn. Reson. Open* **14**, 100090 (2023).

14. Gauthier, J. R. et al. Steady state free precession NMR without fourier transform: RedeFINING THE CAPabilities of ¹⁹F NMR AS A DIS-COVERY Tool. *Angew. Chem. Int. Ed. Engl.* **64**, e202422971 (2025).

15. Chavhan, G. B., Babyn, P. S., Jankharia, B. G., Cheng, H.-L. M. & Shroff, M. M. Steady-state MR imaging sequences: Physics, classi-fication, and clinical applications. *Radiographics* **28**, 1147–1160 (2008).

16. Bieri, O. & Scheffler, K. Fundamentals of balanced steady state free precession MRI. *J. Magn. Reson. Imaging* **38**, 2–11 (2013).

17. https://en.wikipedia.org/wiki/Steady-state_free_precession_imaging.

18. Hennig, J. Echoes—how to generate, recognize, use or avoid them in MR-imaging sequences. Part II: Echoes in imaging sequences. *Concepts Magn. Reson.* **3**, 179–192 (1991).

19. Weigel, M. Extended phase graphs: Dephasing, RF pulses, and echoes - pure and simple. *J. Magn. Reson. Imaging* **41**, 266–295 (2015).

20. Peters, D. C. et al. Improving deuterium metabolic imaging (DMI) signal to noise ratio by spectroscopic multi-echo bSSFP: A pan-creatic cancer investigation. *Magn. Reson. Med.* **86**, 2604–2617 (2021). Cover page of November issue.

21. Montrazi, E. et al. Denoising and joint processing of the kinetic and spectral dimensions enable sub-mM deuterium metabolic imaging characterizations of pancreatic cancer, *NMR Biomedicine*, e4995 (2023). Supplementary cover of November Issue.

22. He, T., Zur, Y., Montrazi, E. T. & Frydman, L. Phase-incremented steady-state free precession as an alternate route to high-resolution NMR. *J. Am. Chem. Soc.* **146**, 3615–3621 (2024).

23. Zur, Y., Stokar, S. & Bendel, P. An analysis of fast imaging sequences with steady-state transverse magnetization refocusing. *Magn. Reson. Med.* **6**, 175–193 (1988).

24. Zur, Y., Wood, M. L. & Neuringer, L. J. Motion-insensitive, steady-state free precession imaging. *Magn. Reson Med.* **16**, 444–459 (1990).

25. Matlab Signal Processing Toolbox, Natick, Massachusetts: The MathWorks Inc.; 2022.

26. Tibshirani, R. Regression shrinkage and selection via the lasso. *J. R. Stat. Soc. Series B*, 267–288, (1996).

27. Beck, A. & Teboulle, M. A fast iterative shrinkage-thresholding algorithm for linear inverse problems. *SIAM J. Imaging Sci.* **2**, 183–202 (2009).

28. https://en.wikipedia.org/wiki/Lasso_(statistics).

29. Mobli, M. & Hoch, J. C. Maximum entropy spectral reconstruction of nonuniformly sampled data. *Concepts Magn. Reson.* **32**, 436–448 (2008).

30. Kazimierczuk, K. & Orekhov, V. Y. Accelerated NMR spectroscopy by using compressed sensing. *Angew. Chem. Int. Ed. Engl.* **123**, 5670–5673 (2011).

31. Lustig, M., Donoho, D. & Pauly, J. M. Sparse MRI: the application of compressed sensing for rapid MR imaging. *Mag. Res. Med.* **58**, 1182–1195 (2007).

32. Reed, G. D. et al. High resolution ¹³C MRI with hyperpolarized urea: In vivo T₂ mapping and ¹⁵N labeling effects. *IEEE Trans. Med. ima-ging* **33**, 362–371 (2013).

33. See for instance https://developers.google.com/machine-learning/crash-course/overfitting/transforming-data, or https://www.youtube.com/playlist?list=PLblh5JKOoLUICTaGLRoHQDuF_7q2GfuJF for good introductory explanations on this matter.

34. Bickel, P. J., Ritov, Y. & Tsybakov, A. B. Simultaneous analysis of Lasso and Dantzig selector. *Ann. Stat.* **37**, 1705–1732 (2009).

35. Wild, J. M. et al. Steady-state free precession with hyperpolarized 3He: experiments and theory. *J. Magn. Reson.* **183**, 13–24 (2006).

36. Leupold, J., Månsson, S., Petersson, S., Hennig, J. & Wieben, O. Fast multiecho balanced SSFP metabolite mapping of 1H and hyperpo-larized 13C compounds. *Magn. Reson. Mater. Phys., Biol. Med.* **22**, 251–256 (2009).

37. Gopal, V. et al. Selective spectroscopic imaging of hyperpolarized pyruvate and its metabolites using a single-echo variable phase advance method in balanced SSFP. *Magn. Reson. Med.* **76**, 1102–1115 (2016).

Acknowledgements

Author contributions

Y.Z. and L.F. conceived the project. M.S., T.H., E.M. and L.F. developed methodologies and collected/processed the data. A.L. and Y.Z. con-tributed calculations. All authors discussed the results leading to the final manuscript. L.F. and Y.Z. wrote the paper.

Competing interests

The authors declare no competing interests.

Additional information

Supplementary information The online version contains supplementary material available at https://doi.org/10.1038/s41467-025-61215-0.

Correspondence and requests for materials should be addressed to Yuval Zur or Lucio Frydman.

Peer review information *Nature Communications* thanks the anon-ymous reviewers for their contribution to the peer review of this work. A peer review file is available.

Reprints and permissions information is available at http://www.nature.com/reprints

Publisher's note Springer Nature remains neutral with regard to jur-isdictional claims in published maps and institutional affiliations.